Physics – Uspekhi **57** (5) 512 – 524 (2014)

CONFERENCES AND SYMPOSIA

PACS numbers: **26.65.+t**, 14.60.Pq, 95.55.Vj

100th ANNIVERSARY OF THE BIRTH OF B M PONTECORVO

Solar neutrino experiments

A V Derbin

DOI: 10.3367/UFNe.0184.201405j.0555

Contents

Abstract. The main results of solar neutrino experiments are presented, ranging from the pioneering Cl – Ar experiment up to the most recent Borexino data. Solar neutrino fluxes and spectra are given for two versions of the standard solar model, and radiochemical and electronic detectors are briefly described. The results of ^{7}Be- and pep-neutrino detection by Borexino are presented. The LMA-MSW oscillation solution of the solar neutrino problem is considered.

1. Introduction

At present, the existence of neutrino oscillations is not in doubt — the active neutrinos ν_e, ν_μ, and ν_τ that are produced or that disappear in a reaction or in a decay are excluded from the states with a certain mass. They are related to the mass states ν_1, ν_2, and ν_3 by the Pontecorvo–Maki–Nakagawa–Sakata (PMNS) matrix [1–3]. Moreover, both the three mixing angles θ_{12}, θ_{23}, and θ_{13} determining the elements of the PMNS matrix, and two mass squared differences $\delta m^2_{12} = m^2_2 - m^2_1$ and $\delta m^2_{32} = m^2_3 - m^2_2$ are also known with a good precision.

Solar neutrinos played a key role in the discovery of neutrino oscillations. The nontrivial problem of the 'deficit' of solar neutrinos, formulated owing to the Cl – Ar experiment performed by R Davis 45 years ago [4], was successfully resolved thanks to the experimental results obtained with the detectors Kamiokande (Kamioka Nucleon Decay Experiment) [5], SAGE (Soviet–American Gallium Experiment) [6], GALLEX/GNO (GALLium EXperiment/Gallium Neutrino Observatory) [7], Super-Kamiokande (Super-Kamioka Neutrino Detection Experiment) [8, 9], and SNO (Sudbury Neutrino Observatory) [10, 11], and to theoretical predictions of neutrino oscillations in a vacuum [12, 13] and in matter [14–18]. The data gathered from solar neutrino detectors, together with the results of reactor antineutrino registration obtained in the KamLAND (Kamioka Liquid-scintillator Anti-Neutrino Detector) experiment [19], permitted determining the mixing parameters θ_{12}, δm^2_{12} and selecting the oscillation solution with a large mixing angle that takes into account the influence of solar matter on neutrino oscillations [Large Mixing Angle (LMA) Mikheyev–Smirnov–Wolfenstein (MSW) solution: LMA-MSW solution]. The Borexino detector has convincingly revealed the validity of the standard solar model (SSM) by demonstrating the existence of ^{7}Be- and pep-neutrinos [20, 21] and confirming the LMA-MSW solution.

At present, solar neutrino detectors are applied in resolving important problems related both to tests of the

A V Derbin B P Konstantinov Petersburg Nuclear Physics Institute, Orlova roshcha, 188300 Gatchina, Leningrad region, Russian Federation
Tel. +7 (81371) 4 63 27
E-mail: derbin@pnpi.spb.ru

Received 6 December 2013
Uspekhi Fizicheskikh Nauk **184** (5) 555 – 567 (2014)
DOI: 10.3367/UFNr.0184.201405j.0555
Translated by G Pontecorvo; edited by A Radzig

modern theory of the solar internal structure and to elementary particle physics.

The most important problem for astrophysics consists in determining the content of chemical elements heavier than helium in the Sun (its metallicity). The fluxes of solar neutrinos depend on its metallicity. Measurement of neutrino fluxes with an accuracy permitting us to distinguish between solar models with high and low metallicities is an issue of top priority.

For particle physics, it is of value to measure the dependence of the electron neutrino registration probability on the neutrino energy — $P_{ee}(E_\nu)$. This dependence, determined by the Mikheyev–Smirnov–Wolfenstein mechanism, is sensitive to nonstandard interactions of neutrinos with electrons and nucleons, which depend upon the neutrino flavor.

Another vital issue is in the precise measurement of the spectrum of recoil electrons produced in pp- and ^{7}Be-neutrino scattering. The shape of the spectrum is extremely sensitive both to the effective neutrino magnetic moment and to nonstandard interactions. The precision that can be reached in experiments with solar neutrinos amounts up to the level sufficient for attaining a sensitivity to the effective neutrino magnetic moment, comparable to the sensitivity of laboratory experiments with reactor neutrinos or neutrinos from artificial sources.

Detectors of solar neutrinos, with which the drastic background reduction necessary for neutrino registration was achieved, were immediately demanded in searching for other rare processes: 2β-decay, neutrino oscillations into a sterile state, the registration of geoneutrinos, and the interaction of dark matter particles with matter.

2. Solar neutrino fluxes and spectra in the standard solar model

The Sun produces energy by transforming hydrogen into helium [22]. The entire fusion reaction can be written as

$$4p \rightarrow {}^4He + 2e^+ + 2\nu_e\,. \tag{1}$$

The total energy released, when four protons are transformed into a helium nucleus, amounts to 26.73 MeV, of which 0.6 MeV is carried away by the neutrinos. Most of the energy (99%) is produced in reactions of the pp-chain; the carbon–nitrogen–oxygen (CNO) cycle contributes about 1% [23, 24]. Neutrinos are emitted in five different reactions of the pp-cycle, and in three reactions of the CNO-cycle.

2.1 Reactions of the pp-chain

The chain of pp-reactions starts with the fusion of two protons into a deuterium nucleus:

$$p + p \rightarrow d + e^+ + \nu_e\,. \tag{2}$$

The transformation of a proton into a neutron is due to the weak interaction; therefore, the rate of reaction (2) is low — about 14 billion years is required for a proton to produce a deuterium nucleus. Precisely reaction (2) determines the rate at which the Sun burns up. The energy spectrum of the emitted electron neutrinos, termed pp-neutrinos, is continuous, with a boundary energy equal to 420 keV.

An alternative mechanism exists for the production of deuterons:

$$p + e + p \rightarrow d + \nu_e\,. \tag{3}$$

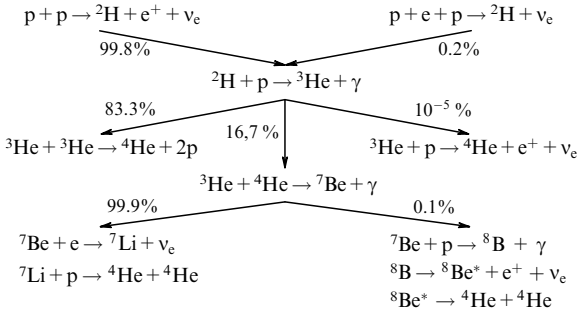

Figure 1. Five different neutrinos (pp, pep, hep, ^{7}Be, and ^{8}B) are emitted in reactions of the pp-chain.

The rate of reaction (3) with three particles in the initial state is about one-four hundredth the rate of the main reaction (2). The energy of the pep-neutrino is fixed — 1.44 MeV.

The deuterium produced nearly instantaneously ($\tau = 6$ s) captures a proton and transforms into helium-3:

$$p + d \rightarrow {}^3He + \gamma\,. \tag{4}$$

Here, a γ-quantum is emitted with the energy $E_\gamma \approx 5.49$ MeV. Since the reaction rate is large, the concentration of deuterium inside the Sun is small, and the direct fusion reaction of two deuterium nuclei into ^{4}He hardly occurs.

The ^{3}He nucleus produced can follow three paths of further transformations (Fig. 1). In most cases (≈ 83%), two ^{3}He nuclei fuse into an ^{4}He nucleus, emitting two protons and releasing 12.86 MeV of kinetic energy:

$$^3He + {}^3He \rightarrow {}^4He + 2p\,. \tag{5}$$

Another possibility, which is realized in approximately 17% cases, is related to the production of a ^{7}Be nucleus:

$$^3He + {}^4He \rightarrow {}^7Be + \gamma\ (E_\gamma = 1.59\ \text{MeV})\,. \tag{6}$$

Finally, there is a small probability ($\sim 10^{-5}$%) of a reaction occurring due to weak interaction:

$$^3He + p \rightarrow {}^4He + e^+ + \nu_e\,. \tag{7}$$

The hep-neutrinos produced here are the most energetic solar neutrinos (their boundary energy amounts to 18.7 MeV), however, their flux is still too small to be registered.

Two versions of transformation exist for the ^{7}Be nucleus. Electron capture results in the production of an ^{7}Li nucleus, which decays into two α-particles upon capturing a proton:

$$^7Be + e \rightarrow {}^7Li + \nu_e\ (E_\nu = 0.862\ \text{MeV})\,, \tag{8}$$

$$^7Li + p \rightarrow {}^4He + {}^4He\ (Q = 17.45\ \text{MeV})\,, \tag{9}$$

where Q is the energy released in the reaction. The energy of monochromatic ^{7}Be-neutrinos is equal to 862 keV (89.6%) or 384 keV (10.4%) if the ^{7}Be nucleus decays into the first excited state of the ^{7}Li nucleus.

Another possibility for the ^{7}Be nucleus transformation, realized in 0.1% cases, involves the capture of a proton:

$$^7Be + p \rightarrow {}^8B + \gamma\ (Q = 0.136\ \text{MeV})\,, \tag{10}$$

$$^8B \rightarrow {}^8Be^* + e^+ + \nu_e\ (Q = 16.3\ \text{MeV})\,, \tag{11}$$

$$^8Be^* \rightarrow {}^4He + {}^4He\ (Q = 1.6\ \text{MeV})\,. \tag{12}$$

The maximum energy of ^{8}B-neutrinos emitted in the β^+-decay of ^{8}B amounts to 16.3 MeV. Cherenkov solar neutrino detectors are only capable of registering neutrino–electron scattering in the case of ^{8}B-neutrinos owing to the high threshold (> 3.5 MeV) of electron registering.

At present, the spectra of recoil electrons have been measured for ^{8}B-, ^{7}Be-, and pep-neutrinos. One can hope that (ν, e)-scattering will be successfully registered for pp- and CNO-neutrinos in the nearest future.

2.2 CNO-cycle

As was noted above, the CNO-cycle contributes about 1% to the total energy release of the Sun. However, in the case of heavier stars exhibiting a higher temperature in the central region, the contribution of the CNO-cycle may turn out to be determinant. The energy releases in the pp-chain and the CNO-cycle even out at a temperature of about 2×10^7 K [23], which is only 1.3 times higher than the temperature at the center of the Sun.

The main reactions of the CNO-cycle within the Sun are presented in Fig. 2. At higher temperatures, there are several additional cycles. Carbon, which is the most abundant element (after hydrogen and helium) in the Sun, plays the part of a catalyst in the main upper cycle. The first cycle starts with the capture of a proton by the ^{12}C nucleus:

$$^{12}\mathrm{C} + \mathrm{p} \to {}^{13}\mathrm{N} + \gamma \ (Q = 1.94 \text{ MeV}) , \qquad (13)$$

which is liberated again together with an ^{4}He nucleus in the reaction

$$^{15}\mathrm{N} + \mathrm{p} \to {}^{12}\mathrm{C} + {}^4\mathrm{He} \ (Q = 4.97 \text{ MeV}) . \qquad (14)$$

In this cycl, two neutrinos are emitted in β^+-decays of the ^{13}N and ^{15}O nuclei:

$$^{13}\mathrm{N} \to {}^{13}\mathrm{C} + \mathrm{e}^+ + \nu_\mathrm{e} \ (E_\nu = 1.20 \text{ MeV}) , \qquad (15)$$

$$^{15}\mathrm{O} \to {}^{15}\mathrm{N} + \mathrm{e}^+ + \nu_\mathrm{e} \ (E_\nu = 1.73 \text{ MeV}) . \qquad (16)$$

In the second lowest cycle, neutrinos are emitted in the β^+-decay of ^{17}F, but their flux is about one-fiftieth as big:

$$^{17}\mathrm{F} \to {}^{17}\mathrm{O} + \mathrm{e}^+ + \nu_\mathrm{e} \ (E_\nu = 1.74 \text{ MeV}) . \qquad (17)$$

Besides β^+-decays, ^{13}N, ^{15}O, and ^{17}F nuclei may also experience electron capture accompanied by the emission of monochromatic neutrinos, but the probability of such a reaction does not exceed 10^{-3} with respect to the probability of β-decay [25].

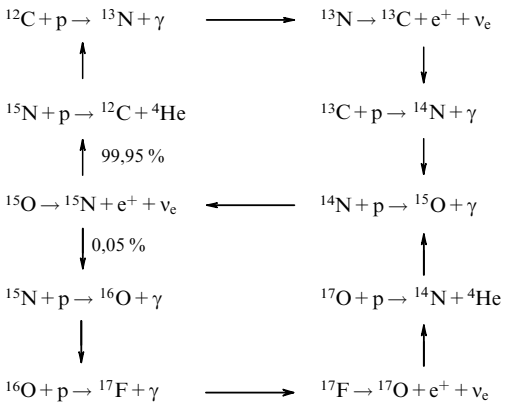

Figure 2. Reactions of the CNO-cycle.

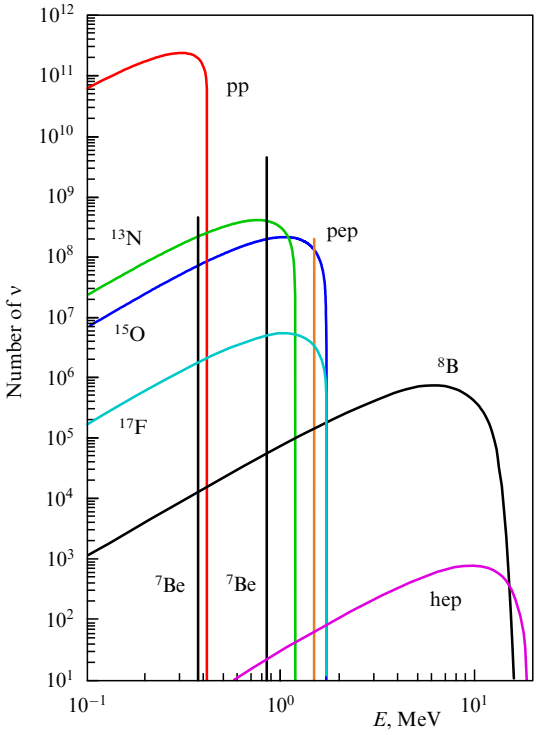

Figure 3. Energy spectra of solar neutrinos (the number of ν per cm^2 MeV s is relevant to continuous spectra, and the number of ν per cm^2 s is relevant to monochromatic spectra).

2.3 Solar neutrino fluxes and spectra

Solar neutrino spectra are shown in Fig. 3, while flux values are presented in Table 1. The pp-neutrino flux of the highest intensity amounts to 6×10^{10} cm^{-2} s^{-1}, about an order of magnitude higher than the flux of ^{7}Be-neutrinos, namely, 5×10^9 cm^{-2} s^{-1}; the ^{8}B-neutrino flux is one-thousandth as big as the flux of ^{7}Be-neutrinos: 6×10^6 cm^{-2} s^{-1}. For comparison, the flux of neutrinos (antineutrinos) from a reactor of thermal power equal to 3 GW at a distance of 15 m amounts to 2×10^{13} cm^{-2} s^{-1}.

In the case of the pp-chain, theoretical SSM uncertainties amount to values from 0.6% to 14%. The difference in the predictions of models involving low or high metallicity

Table 1. Neutrino fluxes in the case of high metallicity (HM) [Grevess, Sauval (1998) (GS98)] [26] and low metallicity (LM) [Serenelli, Basu, Ferguson (2009) (SBF09)] [27] in the Serenelli–Haxton–Pena-Gray model (2011) (SHP11) [24].

Sort of ν	R, cm^{-2} s^{-1}	HM	LM	σ, %	δ, %
pp	10^{10}	5.98	6.03	0.6	0.8
pep	10^8	1.44	1.47	1.2	2.1
hep	10^3	8.04	8.31	30	3.4
^{7}Be	10^9	5.00	4.56	7	8.8
^{8}B	10^6	5.58	4.59	14	17.7
^{13}N	10^8	2.96	2.17	14	26.7
^{15}O	10^8	2.23	1.56	15	30.0
^{17}F	10^6	5.52	3.40	17	38.4

Note: R represents a factor for fluxes relevant to HM and LM, σ is the error in HM and LM flux values, and δ is the relative difference between the HM and LM fluxes.

amounts to 9% in the case of ^{7}Be-neutrinos, 18% in the case of ^{8}B-neutrinos, and 40% for CNO-neutrinos. This is due to the fact that the rate of nuclear reactions depends on the nuclear density and temperature, whose distributions along the solar radius are influenced by the metallicity.

3. Brief chronology of the detection of solar neutrinos

The first weak interaction theory — the theory of the β-decay — was created by E Fermi soon after W Pauli voiced the hypothesis of the existence of the neutrino in 1930. The pioneering experiments, in which the momenta of recoil nuclei experiencing β-decay were measured by A Leipunsky in 1936 and K-capture was realized by D Allen in 1942, indirectly confirmed the existence of the neutrino. Applying Fermi's Lagrangian and the experimentally determined value of the Fermi constant $G_{\rm F}$, H Bethe and R Peierls predicted an exceptionally small ($\sim 10^{-44}$ cm^2) interaction cross section of 1-MeV neutrinos with nuclei [28].

In 1946, B Pontecorvo proposed taking advantage of the ^{37}Cl$(\nu, e)^{37}$Ar reaction for the registration of neutrinos [29]. The notion of the antineutrino arose as a purely theoretical idea, since a neutrino with no electric charge could be a truly neutral particle. Such a neutrino was first proposed by E Majorana in 1937. To resolve this problem, B Pontecorvo proposed in 1946 searching for the reaction of inverse electron capture (EC) on the ^{37}Cl nucleus in a beam of reactor neutrinos (antineutrinos). Indeed, the reactor experiment performed by R Davis in 1955 met with no success in searches for the ^{37}Cl$(\nu, e)^{37}$Ar reaction, which proved the neutrino emitted in the β-decay and the one emitted in the electron capture reaction differ from each other. The discovery by Lee and Yang [30] and Wu et al. [31] in 1957 of the nonconservation of spatial parity gave rise to a new question: is the absence of a signal in the Cl–Ar experiment only related to the neutrino and antineutrino helicities differing from each other, or is it due to the properties of these particles with respect to charge conjugation being different? This question has yet to be answered. The discovery of neutrinoless double beta-decay would point to the neutrino being a Majorana particle.

The possibility of registering solar neutrinos really started to be discussed after it was revealed in 1958 that the cross section of the reaction $^{3}\mathrm{He} + {}^{4}\mathrm{He} \to {}^{7}\mathrm{Be} + \gamma$ was 1000 times larger than previously assumed. Consequently, the production rate of ^{8}B in the reaction $^{7}\mathrm{Be} + \mathrm{p} \to {}^{8}\mathrm{B} + \gamma$ and the flux of ^{8}B-neutrinos also turned out to be 10^3 times higher [32].

The first calculations of ^{7}Be- and ^{8}B-neutrino fluxes were performed by J Bahcall in 1962–1963. In 1964, R Davis proposed a concrete Cl–Ar detector for the registration of solar neutrinos. In 1964–1967, F Reines made an attempt to register (ν, e)-scattering of solar neutrinos. In 1965, V A Kuz'min proposed taking advantage of the reaction ^{71}Ga$(\nu, e)^{71}$Ge, whose energy threshold equals 233 keV, for the registration of solar neutrinos [33].

Practically at the same time as the first results of the R Davis Cl–Ar experiment were reported, a well-known work was published by V Gribov and B Pontecorvo [12], from which it followed that, in order to explain the results of the Cl–Ar experiment, it was required that the mixing angle be close to its maximum value. At the time, the fact that the neutrino mixing angle is larger than in the quark sector seemed to be quite improbable from a theoretical point of view. We now know that this angle is indeed large: $\theta_{12} = 34^\circ$.

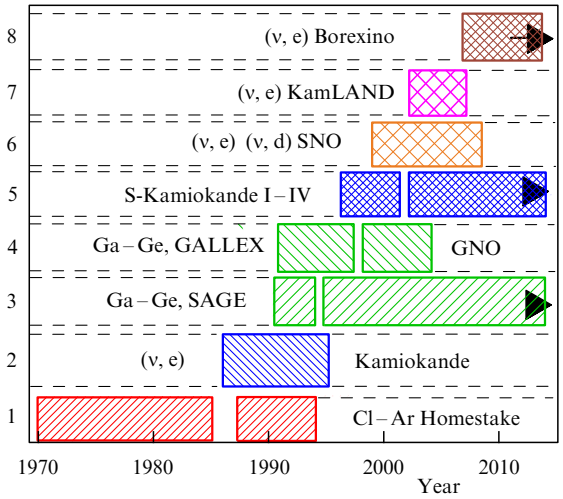

Figure 4. Chronology of the appearance of detectors registering solar neutrinos.

In 1985, another famous study was published by S Mikheev and A Smirnov concerning neutrino oscillations in matter [16]. On the basis of earlier work by Wolfenstein [14, 15], Mikheev and Smirnov [16–18] showed that a mechanism of resonant enhancement of oscillations in matter is possible, which in the case of a low vacuum mixing, $\theta_{12} \sim 10^{-2}$, leads to a large conversion probability of the electron neutrino into the muon neutrino inside solar matter. This mechanism also explained the results of the Cl–Ar experiment in the case of the conventionally adopted assumption that vacuum mixing is small. As it turned out, studies [12, 16–18] resolve the problem of solar neutrinos. But it was necessary to create eight solar neutrino detectors (Fig. 4) in order to achieve such an understanding. The main results obtained with these detectors are presented in Table 2.

4. Radiochemical experiments

Two kinds of radiochemical detectors registered solar neutrinos: chlorine (Cl–Ar), and gallium (Ga–Ge). The main parameters of radiochemical detectors are shown in Table 3.

4.1 Cl–Ar detectors

The reaction of inverse electron capture, $\nu_e + {}^{37}\mathrm{Cl} \to {}^{37}\mathrm{Ar} + \mathrm{e}^-$, proposed by Pontecorvo [29], was tapped for the registration of neutrinos. The ^{37}Ar produced was extracted from 615 t of perchloroethylene and its radioactivity was counted by a low-background gas counter. The measured production rate of ^{37}Ar [5 atoms in 1 month in 615 t of C_2Cl_4 or 2.5 SNU (solar neutrino unit — 1 neutrino capture every 10^{36} target nuclei per s)] amounted to $\sim 1/3$ of the SSM prediction. This is how the solar neutrino problem arose, and it was resolved 30 years later.

4.2 Ga–Ge detectors

Neutrino registration in the SAGE and GALLEX/GNO experiments is based on utilization of the reaction proposed by Kuz'min [33]: $\nu_e + {}^{71}\mathrm{Ga} \to {}^{71}\mathrm{Ge} + \mathrm{e}^-$. The reaction threshold amounted to only 233 keV, which permits registering most of the pp-neutrinos, the contribution of which to the

Table 2. Solar neutrino detectors and the principal results.

Detector	Principal result
Cl – Ar	First registration of solar neutrinos. Formulation of the problem of the solar neutrino flux deficit
Kamiokande	First real-time registration of neutrinos. Confirmation of the signal arrival from the Sun
SAGE, GALLEX/GNO	Registration of pp-neutrinos composing the main part of the solar neutrino flux. Confirmation of the registered flux deficit as opposed to the SSM prediction
Super-Kamiokande	Precision measurement of the ^{8}B-neutrino flux. Discovery of atmospheric neutrino oscillations
SNO	Discovery of solar neutrino oscillations. Measurement of ^{8}B-neutrino flux in charged and neutral channels
KamLAND	Discovery of reactor neutrino oscillations. Choice of the LMA oscillation solution for antineutrinos
Borexino	Measurement of ^{7}Be- and pep-neutrino fluxes. The LOW oscillation solution* for neutrinos was excluded
* LOW — Long Oscillation Wavelength.	

Table 3. Characteristics of radiochemical detectors.

Detector	Duration of experiment	Composition, mass of detector	Method, registered neutrinos	Registration threshold, keV	Result *
Homestake	1970 – 1994, 108 cycles	C_2Cl_4, 615 t	$\nu_e + {}^{37}Cl \to {}^{37}Ar + e^-$, ^{7}Be (13.1%) + pep (2.7%) + CNO (2.4%) + ^{8}B (81.8%)	814	$2.56 \pm 0.16 \pm 0.16$ SNU, 0.322 ± 0.080
SAGE (in operation)	1990 – 2006, 157 cycles	Ga (metal), 50 t	$\nu_e + {}^{71}Ga \to {}^{71}Ge + e^-$, pp (55%) + ^{7}Be (28.3%) + pep (2.3%) + CNO (3.4%) + ^{8}B (11%)	233	$65.4 \pm 3.1 \pm 2.7$ SNU, 0.511 ± 0.075
GALLEX	1991 – 1997, 67 cycles	$GaCl_3$, 30.3 t			$73.4 \pm 6.1 \pm 4.1$ SNU, 0.574 ± 0.098
GNO-30	1998 – 2003, 58 cycles				$62.9 \pm 5.4 \pm 2.5$ SNU, 0.492 ± 0.081
GALLEX + GNO					$67.6 \pm 4.0 \pm 3.2$ SNU, 0.529 ± 0.079
* Measured counting rate (in SNU) and ratio of measured counting rate to the value expected in SHP11(GS98) SSM [24].					

common counting rate of solar neutrinos was 55% (see Table 2). An important advantage of a gallium detector also consists in the shorter lifetime (16.5 days) of ^{71}Ge against 50.6 days for ^{37}Ar, which permits extracting Ge from the detector volume more often.

The GALLEX and GNO experiments were carried out in the GRAN SASSO laboratory [3500-meter water equivalent (m.w.e.)] in 1991–2003 with a detector having a mass of 30 t [7, 34–36].

The SAGE experiment in the Baksan Neutrino Observatory (4700 m.w.e.) was initiated in 1991 and at present measurements are still under way [6, 37]. The mass of gallium in the SAGE detector is twice the mass in GALLEX/GNO. In spite of the existing difference in the methods of extracting Ge from the enormous mass of gallium, the results of SAGE and GALLEX/GNO experiments for the counting rate turn out to coincide within the limits of experimental errors. This served as an additional confirmation of neutrino registration. SAGE and GALLEX confirmed the deficit of neutrinos, but the ratio of the registered flux to the expected value was 0.55 instead of 0.3, as in the Cl – Ar experiment.

An important merit of the SAGE and GALLEX detectors consists in the fact that they were calibrated with a ^{51}Cr source of neutrinos. In 2004, the SAGE detector was additionally calibrated utilizing an ^{37}Ar source. It is interesting that the number of events registered from the neutrino sources turned out to be lower than the expected value with a statistical significance of 3σ [38]. This may be related to the electron neutrino oscillating into a sterile state. The region of possible oscillation parameters (the mass squared difference δm_s^2 and the mixing angle θ_s) turned out to be compatible with the parameters found in accelerator and reactor experiments [39]. To search for such transitions, the proposal was made to place a ^{51}Cr source at the center of the Ga-detector divided into two concentric zones. The experiment is sensitive to oscillations with $\delta m^2 \sim 1$ eV^2 with the amplitude of $\sin^2(2\theta_s)$ oscillations of several percent [40].

5. Experiments with real-time electronic detectors

The main parameters of the five electronic detectors are presented in Table 4. Kamiokande, Super-Kamiokande, and SNO relate to the category of Cherenkov detectors, while KamLAND and Borexino to scintillation detectors.

5.1 Kamiokande-II: the first Cherenkov detector

The Kamiokande-II detector was situated in the Kamioka mine (2700 m.w.e.). It was initially supposed to be used for searching the proton decays. The detector was a cylinder 15.6 m in diameter and 16 m high filled with 3000 t of purified water viewed by 1000 photomultiplier tubes (PMTs) mounted on the surface of the tank. Owing to the high degree of purification of the water, it turned out to be possible to lower the electron registration threshold to 7.5 MeV and to first register neutrinos from the supernova SN1987A and then solar ^{8}B-neutrinos. Reconstruction of the direction of motion of the recoil electrons, making use of

Table 4. Characteristics of electronic detectors.*

Detector		Duration of experiment	Composition, mass of detector	Method, registered neutrinos	Registration threshold, MeV	$R = \Phi_{meas}/\Phi_{SHP11(GS98)}$, Φ, 10^6 cm^{-2} s^{-1}
Kamiokande-II		1986 – 1995	H_2O, 3 kt	$\nu + e^- \to \nu + e^-$ ^{8}B (100%)	7.5	$R_{8B} = 0.50 \pm 0.07$ $\Phi_{\nu e} = 2.80 \pm 0.38$
Super-Kamiokande	I	1996 – 2001, 1496 days	H_2O, 50 kt, 32 kt — IV, 18 kt — OV	$\nu + e^- \to \nu + e^-$ ^{8}B (100%)	5.5	$R_{8B} = 0.43 \pm 0.01$ $\Phi_{\nu e} = 2.38 \pm 0.08$
	II	2002 – 2005, 791 days				$R_{8B} = 0.43 \pm 0.03$ $\Phi_{\nu e} = 2.41 \pm 0.16$
	III	2006 – 2008, 548 days			5.0	$R_{8B} = 0.42 \pm 0.01$ $\Phi_{\nu e} = 2.32 \pm 0.06$
	IV	Since 2008			4.5	$R_{8B} = 0.42 \pm 0.01$ $\Phi_{\nu e} = 2.34 \pm 0.05$
SNO	I	1999 – 2001	D_2O, 1006 t	$\nu_e + d \to p + p + e^-$ CC **, 4 MeV	6.5	$R_{8B} = 0.32 \pm 0.02$ $\Phi_{CC} = 1.76 \pm 0.11$
				$\nu_X + d \to p + n + \nu_X$ NC, 2.22 MeV		$R_{8B} = 0.43 \pm 0.05$ $\Phi_{\nu e} = 2.39 \pm 0.27$
				$\nu_X + e^- \to \nu_X + e^-$ ES ***		$R_{8B} = 0.91 \pm 0.11$ $\Phi_{NC} = 5.09 \pm 0.62$
	II	2001 – 2004, 391 days	+ NaCl 2 t	$^{35}Cl + n \to {}^{36}Cl + 8.6$ MeV $(2-4\gamma)$		$\Phi_{CC} = 1.68 \pm 0.11$ $\Phi_{\nu e} = 2.35 \pm 0.27$ $\Phi_{NC} = 4.94 \pm 0.43$
	III	2004 – 2006	+ ^{3}He counters	$^3He + n \to p + {}^3H$ +0.76 MeV		$\Phi_{CC} = 1.67 \pm 0.09$ $\Phi_{\nu e} = 1.77 \pm 0.24$ $\Phi_{NC} = 5.54 \pm 0.45$
	I + II + III, fit for all reactions					$R_{8B} = 0.94 \pm 0.04$ $\Phi_B = 5.25 \pm 0.20$
KamLAND		2002 – 2007	Dodecane 0.8, PC 0.2, 1000 t	$\nu + e^- \to \nu + e^-$ ^{8}B (100%)	5.5	$R_{8B} = 0.50 \pm 0.07$ $\Phi_B = 2.77 \pm 0.41$
Borexino				$\nu + e^- \to \nu + e^-$ ^{7}Be (0.862 MeV) pep ^{8}B (> 3 MeV)	0.2	$R_{7Be} = 0.62 \pm 0.04$ 46 ± 2.2 events per day in 100 t $R_{pep} = 0.69 \pm 0.16$ 3.1 ± 0.7 events per day in 100 t $R_{8B} = 0.43 \pm 0.08$ 0.22 ± 0.04 events per day in 100 t

* Φ is the registered ^{8}B-neutrino flux, and R is the ratio of the measured counting rate to the value expected in the SHP11(GS98) SSM [24].
** Charged current.
*** (ν, e)-scattering.

the cone of Cherenkov radiation, revealed the Sun to be the source of neutrinos [5].

The first result of Kamiokande-II was published before the data from the Ga–Ge detectors were obtained. The difference in the ratios of the measured neutrino counting rates to the expected values, $R = \Phi_{meas}/\Phi_{SSM}$, for Kamiokande-II and for the Cl–Ar detector differs from zero by 1.3σ. This was the first indication of the dependence of the solar neutrino deficit on the neutrino energy.

5.2 Super-Kamiokande: a large Cherenkov water detector

The success achieved with Kamiokande-II in neutrino physics and the negative result of the search for proton decay led to the creation of the Super-Kamiokande (SK) detector, the mass of which is 17 times larger. Super-Kamiokande is a cylindrical tank of stainless steel whose height (41.4 m) and diameter (39.3 m) are nearly equal to each other and that contains 50 kt of highly purified water. Inside the tank there is also a central (internal) volume (IV) (32 kt) cylindrical in shape that is optically separated from the outer volume. All the PMTs are mounted on the surface of the internal detector: 11 thousand PMTs with photocathodes 20 inches in diameter view the internal volume, and 1800 PMTs with photocathodes 8 inches in diameter view the outer volume (OV). The external detector suppresses the surrounding γ-activity and neutron activity and plays the part of a muon prohibition (veto). The Super-Kamiokande collaboration initiated measurements in 1996 and already after a lapse of two years it announced the discovery of atmospheric neutrino oscillations [41].

Chronologically, operation of the detector is divided into four periods: SK-I, SK-II, SK-III, and SK-IV (see Table 4) [9]. The end of the first period was marked by the simultaneous destruction of 6600 PMTs caused by a hydrau-

lic shock. Period SK-III ensued upon total reconstruction of all the PMTs. Period SK-IV corresponds to the beginning of operation of the new electronics and, in particular, to the registration of accelerator neutrinos in the T2K (Tokai to Kamioka) experiment. During the 17 years of running the Super-Kamiokande experiment, the electron registration threshold was lowered from 5.5 MeV to ≈ 3.5 MeV.

The result produced in SK-I confirmed the deficit of solar ^{8}B-neutrinos, and, here, the flux of ^{8}B-neutrinos was measured with a precision of 3.4% [8].

5.3 SNO: a detector with heavy water

The Canadian underground science laboratory SNO is located 2 km below the surface or at a depth of 6000 m.w.e. in the mine near Sudbary, Ontario. The detector of the same name contains 1 kt of heavy water (D_2O) filling the acrylic sphere 12 m in diameter. The sphere is viewed by 9500 PMTs mounted on an open-work construction 17 m in diameter, which provides a 60% geometrical efficiency. The cavity housing the acrylic sphere is filled with 70 kt of natural water for supporting the sphere and suppression of the external γ- and n-activities.

Besides the events of neutrino–electron scattering, the SNO detector registers two neutrino interactions with the deuteron:

$$\nu_e + d \to p + p + e^-\,, \tag{18}$$

$$\nu_{e,\mu,\tau} + d \to p + n + \nu_{e,\mu,\tau}\,. \tag{19}$$

The first reaction proceeds via the charged current and is only caused by the electron neutrino, while the second proceeds via the neutral current and is caused by neutrinos of any flavor.

The SNO detector was in operation starting from May 1999 until November 2006. The first measurements with the detector filled with pure D_2O were published in 2001 [42] and revealed the flux of neutrinos registered in the neutral-current reaction (19) to correspond to SSM predictions. The flux of ^{8}B-neutrinos registered via the charged current channel (18) amounted to 1/3 of the magnitude predicted by SSM [43]. Thus, the existence of neutrino oscillations involving a change in flavor was demonstrated quite clearly.

During the second phase of the experiment, 2 t of salt (NaCl) was dissolved in the detector water for enhancement of the registration efficiency of neutrons produced in reaction (19) with the neutral current. The ^{35}Cl nucleus exhibits a large neutron capture cross section, and prompt γ-quanta are emitted here with an energy of 8 MeV [10].

In the final, third, phase of the experiment, an array of 36 ^{3}He counters situated in the heavy water [11] was utilized for registering neutrons. The results of all stages are in agreement with each other (see Table 4). The final fit [44] performed with all the statistics for all reactions yields the following value for the ^{8}B-neutrino flux: $\Phi_B = (5.25 \pm 0.20) \times 10^6$ cm^{-2} s^{-1}, which is in agreement with the prediction of SHP11(GS98) SSM: $\Phi_B = (5.58 \pm 0.78) \times 10^6$ cm^{-2} s^{-1}.

In 2014, operation of the new modification of the detector, SNO+, will deploy. This is a scintillation detector based on linear alkyl benzene, the main goals of which are to register pep neutrinos, SNO-neutrinos, and geoneutrinos, and to search for the neutrinoless double beta-decay of ^{130}Te [45].

5.4 KamLAND: a detector of reactor neutrinos

The KamLAND detector comprises a transparent sphere 132 m in diameter filled with 1 kt of liquid scintillator based on dodecane (80%) and pseudocumene (PC) (20%). The acrylic sphere is viewed by 2100 (17- and 20-inch) PMTs mounted on a sphere of stainless steel 18 m in diameter and providing a 30% geometrical survey. The space between the two spheres is filled with mineral oil. The whole construction is located in a cylindrical water cavity, inside which 225 PMTs are placed for the registration of muons.

The detector was designed for searches of electron antineutrino oscillations at large distances (> 100 km) from the reactor. KamLAND started measurements in January 2002, and in 145 days reported the first result, according to which only 61% of the reactor neutrinos were registered [46]. This corresponded to the oscillation parameters found for solar neutrinos in the LMA solution.

KamLAND presented the results of registering (ν, e)-scattering in the case of solar ^{8}B-neutrinos [47] during the 2002–2007 period. The obtained magnitude of the ^{8}B-neutrino flux, $\Phi = (2.77 \pm 0.26 \pm 0.32) \times 10^6$ cm^{-2} s^{-1}, is consistent with the results obtained by Super-Kamiokande and SNO. Measures aimed at significantly reducing the energy threshold of the detector, nevertheless, did not permit registering ^{7}Be-neutrinos from the Sun.

At present, the KamLAND-Zen (KamLAND: Zero Neutrino) experiment in search for the $2\beta0\nu$-decay of ^{136}Xe is under way: 300 kg of ^{136}Xe is dissolved in a 17-m^3 volume located at the center of a scintillation detector [48].

Another proposed application of the detector is related to the search for electron neutrino oscillations to the sterile state. In the CeLAND project, a 50-kCi ^{144}Ce source is to be placed at the center of the KamLAND detector [49].

6. Borexino: a scintillation detector

The 'youngest' detector of solar neutrinos, Borexino, started data taking [50–52] in May 2007. The experiment is under way at the Gran Sasso Laboratory: the largest underground laboratory both in size and in the number of experiments deployed. Although Gran Sasso is considered an underground laboratory, it is actually situated at a height of 1000 m above sea level in a tunnel under the Apennines, which provides suppression of the muon flux equivalent to the suppression by 3500 m.w.e.

The scintillator [PC + PPO (propylene oxide)] 278 t in mass is located inside a thin nylon sphere that is surrounded by a concentric PC buffer layer 2.6 m thick (Fig. 5). The buffer layer [PC + DMP (dimethoxypropane)] is partitioned by a nylon film, so as to reduce the diffusion of radon into the scintillator bulk. The total PC mass (1200 t) is contained inside a steel sphere 13.7 m in diameter. The scintillation light is collected by 2212 PMTs distributed uniformly over the surface of the sphere. The steel sphere is located within a tank containing 2100 t of purified water which serves as additional shielding against external γ-quanta and neutrons. Two hundred eight PMTs housed inside the tank register the Cherenkov radiation of muons in the water.

Each event in the detector is characterized by the number of fired PMTs for which the pulse amplitudes and arrival times are recorded. These data are used in reconstruction of the event energy and of its spatial coordinates, as well as for particle (e, p, α) identification.

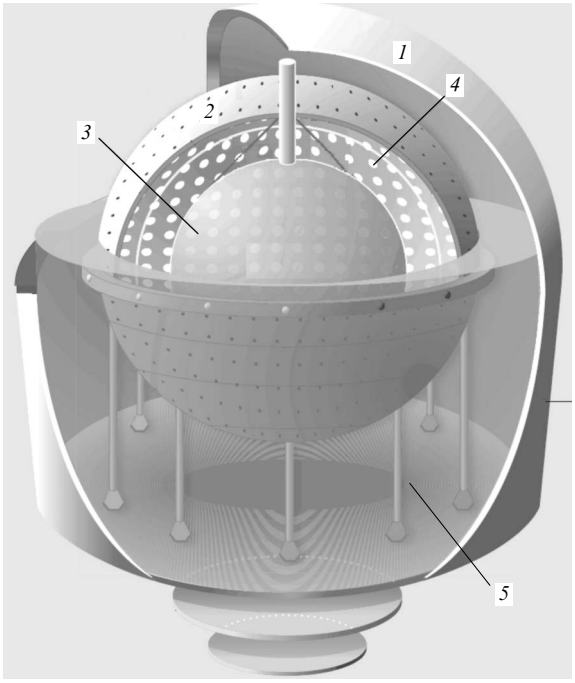

Figure 5. Schematic of the Borexino detector: *1* — tank with water, *2* — steel sphere, *3* — nylon sphere, *4* — photomultiplier tubes, *5* — water shielding. (Taken from Ref. [53].)

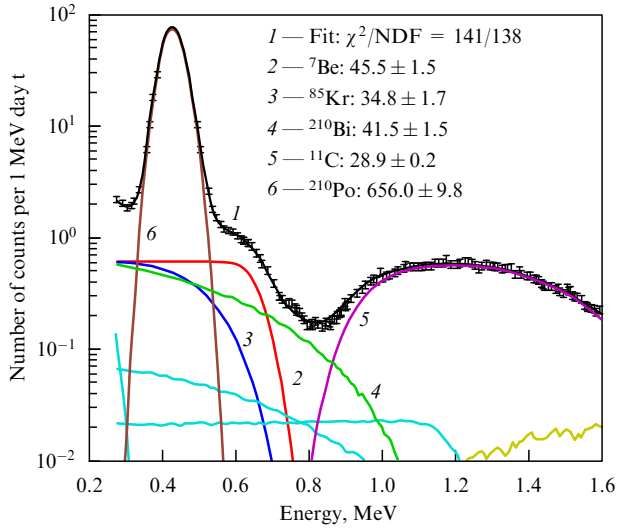

Figure 6. Energy spectrum measured by Borexino in 741 days. The main components of the spectrum are shown. In the case of *2–6* spectra, presented are the numbers of counts per day in 100 t. (Taken from Ref. [20].)

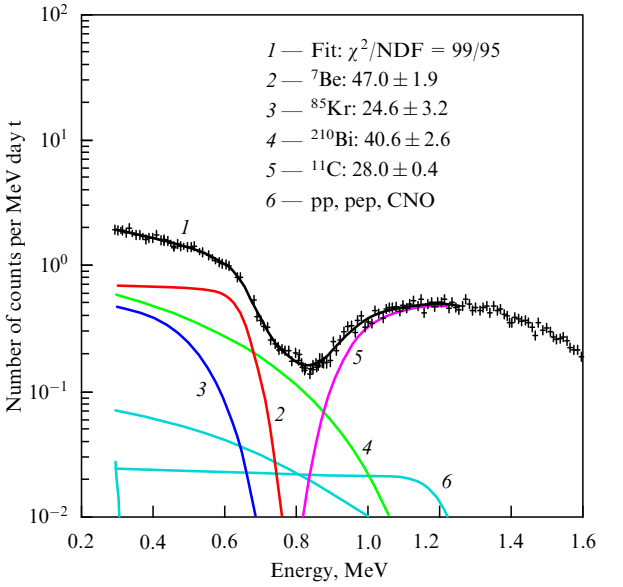

Figure 7. Energy spectrum after deleting the events related to the α-decay of ^{210}Po. In the case of *2–6* spectra, presented are the numbers of counts per day in 100 t. The value of the CNO-neutrino flux was fixed in the fit. (Taken from Ref. [20].)

6.1 Results of measurement of (ν, e)-scattering in the case of ^{7}Be- and ^{8}B-neutrinos

The spectrum in the central part of the detector with a mass of 76 t is shown in Figs 6 and 7 [20]. Events coinciding in time within the limits of 2 ms with the muon veto signal, as well as consecutive events, the time interval between which does not exceed 2 ms, were deleted from the spectrum.

At low energies, the background is determined by the β-decays of ^{14}C ($E_\nu = 156$ keV) nuclei, which actually determine the lower threshold of the energy region accessible to analysis (≈ 200 keV). The pronounced peak at the energy of ≈ 450 keV is related to the α-decay of ^{210}Po nuclei. The decay rate of ^{210}Po is not in equilibrium with the β-decay rate of the preceding ^{210}Bi nucleus.

The dip in the spectrum at the energy of 660 keV corresponds to the origin of the spectrum of recoil electrons in the case of monoenergetic ^{7}Be-neutrino scattering ($E_\nu = 862$ keV). Within the 1.0–2.0 MeV interval, the background is determined by β^+-decays of the ^{11}C isotope ($\tau = 29$ min, $Q = 1.98$ MeV), which is produced from ^{12}C under the action of muons. The production rate of ^{11}C was determined to amount to 29 ± 0.2 nuclei for every 100 t per day. The Borexino background level at energies ~ 1 MeV is no more than 1% the background levels achieved by any other detector.

Determination of the counting rate of ^{7}Be-neutrinos was performed both for the experimental spectrum containing the α-peak due to ^{210}Po decays (see Fig. 6) and for the spectrum with deleted signals from α-particles (see Fig. 7). Both fitting procedures yielded practically the same result. In the case of ^{7}Be-neutrinos (862 keV), Borexino registered 46.0 ± 1.5 (stat.) ± 1.5 (syst.) (ν, e)-scattering events in 100 t of PC per day [20]. The expected counting rate for the nonoscillation solution in the SSM with high metallicity [SHP11(GS98)] [24] amounts to 74.0 ± 5.2 events per day in 100 t, which deviates from the measured value by 5.0σ.

For values of oscillation parameters established for the LMA-MSW solution [54, 55], the ^{7}Be-neutrino flux $\Phi_{^7\mathrm{Be}} = (4.84 \pm 0.24) \times 10^9$ cm^{-2} s^{-1}.

Neutrino scattering on an electron is due to the exchange of W- and Z-bosons, and the electron neutrino undergoes scattering owing to both the charged (W) and the neutral (Z) currents, while μ- and τ-neutrino scattering proceeds only due to the neutral current. As a result, the expected spectrum of recoil electrons is expressed as follows:

$$\frac{\mathrm{d}\sigma}{\mathrm{d}E_\mathrm{e}} = P_\mathrm{ee}\,\frac{\mathrm{d}\sigma}{\mathrm{d}E_\mathrm{e}}\bigg|_{\mathrm{W+Z}} + (1 - P_\mathrm{ee})\,\frac{\mathrm{d}\sigma}{\mathrm{d}E_\mathrm{e}}\bigg|_{\mathrm{Z}}, \qquad (20)$$

where P_ee is the relative number of electron neutrinos.

The survival probability of electron neutrinos at 862 keV determined by Borexino amounts to $P_{ee}(0.862\ \text{MeV}) = 0.51 \pm 0.07$ for predictions by SHP11(GS98) SSM [24].

The ratio of the measured ^{7}Be-neutrino flux to the flux expected in SSM (the reduced flux) amounts to $f_{^7\text{Be}} = 0.97 \pm 0.09$. The values of $f_{^7\text{Be}}$ determined in preceding experiments lay within a broad interval (0–1.27). Thus, the existence of ^{7}Be-neutrinos was first reliably established by the Borexino experiment. The flux of ^{7}Be-neutrinos was measured with a precision of 4.8%.

Inclusion of the data on the ^{7}Be-neutrino flux in the general balance equations for all solar neutrinos significantly improves the accuracy of determining the fluxes of the other neutrinos [56]. Thus, the flux of pp-neutrinos determined, with due account of Borexino data and other solar experiments, from the balance equations under the condition of restricted solar luminosity is

$$\Phi_{pp} = (6.06^{+0.02}_{-0.06}) \times 10^{10}\ \text{cm}^{-2}\ \text{s}^{-1}\,,$$

while the reduced flux $f_{pp} = 1.013^{+0.003}_{-0.01}(1\sigma)$ [20].

Besides the ^{7}Be-neutrinos, it turned out to be possible in the experiment to register (ν, e)-scattering of high-energy ^{8}B-neutrinos [57]. The expected ^{8}B-neutrino counting rate is about 1/200 that for ^{7}Be-neutrinos. The ^{8}B-neutrino counting rate measured, starting from the threshold of 3 MeV, amounted to $0.217 \pm 0.038(\text{stat.}) \pm 0.008(\text{syst.})$ counts per day for every 100 t, which corresponds to the neutrino flux

$$\Phi_{^8\text{B}} = (2.4 \pm 0.4) \times 10^6\ \text{cm}^{-2}\ \text{s}^{-1}$$

and to the survival probability $P_{ee}(8.6\ \text{MeV}) = 0.29 \pm 0.10$. It is important that the relative numbers of electron neutrinos have been determined for the first time in a single experiment for energy intervals with differing degrees of influence of vacuum oscillations and oscillations in matter. The ratio between survival probabilities for ^{7}Be- and ^{8}B-neutrinos, $P_{ee}(^7\text{Be})/P_{ee}(^8\text{B}) = 1.5$, is consistent with the LMA-MSW solution and differs from 1 by 1.8σ, thus indicating that P_{ee} depends on the neutrino energy.

6.2 Registration of pep neutrinos and the upper limit of the CNO-neutrino flux

As noted in Section 2, pep-neutrinos are produced in the reaction of deuterium production. The energy of pep-neutrinos is equal to 1.44 MeV, and the edge of (ν, e)-scattering corresponds to the energy of 1.22 MeV. The main contribution to the background in this region is related to β^+-decays of ^{11}C nuclei ($\tau = 29.4$ min), which are produced owing to the action of muons in the reaction $\mu(^{12}\text{C}, ^{11}\text{C})$n. For suppression of the ^{11}C background, use was made of the coincidence between the muon track and the reconstructed registration point of the 2.2-MeV γ-quantum from neutron capture on hydrogen. By exclusion of all events occurring inside a sphere with a 1-m radius for 30 min, an 11-fold reduction was achieved of the ^{11}C background, while 48.4% of the accumulation time was retained. An additional criterion was related to the selection of events in which the positron produced in β^+-decay of the ^{11}C nucleus forms orthopositronium (o-Ps). The lifetime of o-Ps in a liquid organic scintillator amounts to about 3 ns; registration of the time delay between annihilation quanta and the first scintillation photons permitted additionally lowering the background by a factor of two [21].

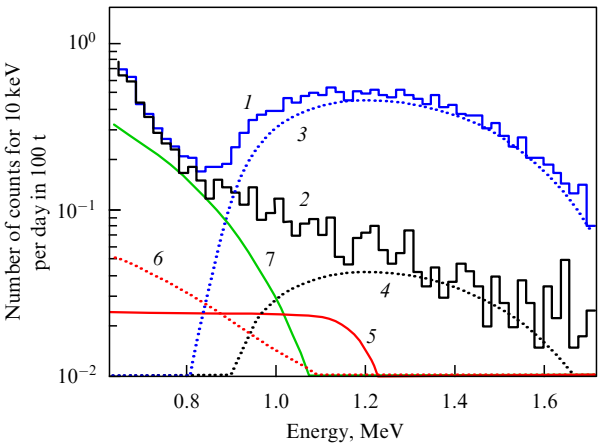

Figure 8. Event spectrum in the central part of the Borexino detector before (*1*) and after (*2*) selection of triple space–time coincidences corresponding to the production and decay of ^{11}C nuclei. Also presented are the contributions to the ^{11}C spectrum before (curve *3*) and after (curve *4*) the selection. Curves *5–7* illustrate the respective contributions from the pep- and CNO-neutrinos and of ^{210}Bi. (Taken from Ref. [21].)

The results of fitting are depicted in Fig. 8 [21]. The counting rate determined amounted to $3.1 \pm 0.6(\text{stat.}) \pm 0.4(\text{syst.})$ events in 100 t per day, which corresponds to a neutrino flux of $(1.6 \pm 0.3) \times 10^8\ \text{cm}^{-2}\ \text{s}^{-1}$ for the LMA-MSW solution and SHP11(GS98) SSM. The electron neutrino observation probability amounts to $P_{ee}(1.44\ \text{MeV}) = 0.62 \pm 0.17$.

At the same time, the most rigorous restriction was imposed on the CNO-neutrino flux: $\Phi_{\text{CNO}} \leqslant 7.7 \times 10^8\ \text{cm}^{-2}\ \text{s}^{-1}$, which is only 1.5 times higher than the flux expected in 5SHP11(GS98) SSM.

6.3 Search for rare processes. The neutrino magnetic moment

The record low background level achieved with the Borexino detector provides for high sensitivity to rare low-energy processes. At present, searches have been performed for magnetic moment of solar neutrinos [51], transitions with violation of the Pauli principle in the ^{12}C nucleus [58], solar and relic antineutrinos [59], solar axions with an energy of 5.5 MeV produced in the reaction $\text{p(d}, ^3\text{He})A$ [60], and a heavy sterile neutrino emitted in the ^{8}B-decay in the Sun [61].

To reveal or to impose an upper bound on the neutrino magnetic moment, advantage was taken of the characteristic energy dependence of the spectrum of recoil electrons in the case of scattering due to the magnetic moment. While the weak scattering cross section tends toward a constant value as the energy E_e of the recoil electron tends to zero, the cross section of magnetic scattering increases as $1/E_e$:

$$\frac{d\sigma}{dE_e} = \pi r_0^2 \mu_{\text{eff}}^2 \left(\frac{1}{E_e} - \frac{1}{E_\nu}\right). \qquad (21)$$

Here, r_0 is the classical electron radius, and E_ν is the neutrino energy.

Since the neutrinos are mixed, it is the effective magnetic moment that is registered in neutrino–electron scattering:

$$\mu_{\text{eff}}^2 = \sum_j \left| \sum_k \mu_{kj} A_k(E_\nu, L) \right|^2, \qquad (22)$$

where μ_{jk} is an element of the matrix of neutrino electromagnetic moments, and $A_k(E_\nu, L)$ is the amplitude of the kth mass state at the scattering point [62]. As for the Majorana neutrino, only the transition moments $\mu_{j\neq k}$ differ from zero, while the diagonal elements μ_{jj} of the matrix are equal to zero. For the Dirac neutrino, all the matrix elements μ_{jk} can differ from zero. The neutrino effective magnetic moment can be represented both in the mass (which is more natural) and in the flavor bases.

For the MSW oscillation solution under the assumption that $\theta_{13} \approx 0$, the effective magnetic moment can be expressed through the magnetic moments of flavor states [63–65]:

$$(\mu^2_{\text{eff}})_{\text{MSW}} = P_{\text{ee}}\mu_{\text{e}}^2 + (1 - P_{\text{ee}})(\cos^2\theta_{23}\,\mu_{\mu}^2 + \sin^2\theta_{23}\,\mu_{\tau}^2)\,. \tag{23}$$

Borexino experiment established an upper bound from the results of measurements performed over 192 days: $|\mu_{\text{eff}}| \leqslant 5.4 \times 10^{-11}\mu_{\text{B}}$, where μ_{B} is the electron Bohr magneton (90% C.L.) [51]. The bound obtained is conservative: when $\mu_{\text{eff}} = 5.4 \times 10^{-11}\mu_{\text{B}}$, nearly 20% of events registered within the energy interval from 230 to 310 keV should be due to (ν, e)-scattering related to the neutrino magnetic moment.

Making use of the most probable values of P_{ee}, θ_{12}, and θ_{23}, one can obtain the following bounds from the condition $\mu_{\text{eff}} \leqslant 5.4 \times 10^{-11}\mu_{\text{B}}$ [52]: for the electron neutrino $\mu_{\nu\text{e}} \leqslant 7.3 \times 10^{-11}\mu_{\text{B}}$, for the muon neutrino $\mu_{\nu\mu} \leqslant 11.4 \times 10^{-11}\mu_{\text{B}}$, and for the τ-neutrino $\mu_{\nu\tau} \leqslant 11.4 \times 10^{-11}\mu_{\text{B}}$. These constraints must be compared with those obtained from reactor and accelerator experiments in which (ν, e)-scattering was studied: $\mu_{\nu\text{e}} < 2.9 \times 10^{-11}\mu_{\text{B}}$ — GEMMA (Germanium Experiment for measurement of Magnetic Moment of Antineutrino) [66], $\mu_{\nu\mu} < 68 \times 10^{-11}\mu_{\text{B}}$ — LSND (Liquid Scintillator Neutrino Detector) experiment [67], and $\mu_{\nu\tau} < 39{,}000 \times 10^{-11}\mu_{\text{B}}$ — DONUT (Direct Observation of NU Tau) experiment [68]. As evidenced by the foregoing, the Borexino result significantly improved the constraints on the magnetic moments of the μ- and τ-neutrinos.

Further plans of the Borexino Collaboration are related to the possible registration of pp- and CNO-neutrinos, to continuation of the accumulation of geoneutrino and reactor antineutrino events, and to the search for rare processes.

The high energy and spatial resolution and low background level of the Borexino detector are a clear advantage in searches for oscillations of the electron neutrinos to a sterile state for mixing parameters $\delta m_{\text{s}}^2 \sim 1\ \text{eV}^2$ and $\sin^2(2\theta_{\text{s}}) \sim 0.1$. At present, an experiment in which artificial neutrino sources (^{51}Cr and ^{144}Pr) will be used is in preparation [69].

7. Neutrino oscillations in a vacuum and in matter

In the most simple case, when the electron neutrino produced in β- or EC-decay represents a superposition of two mass states, namely

$$|\nu_{\text{e}}\rangle = \cos\theta_{12}\,|\nu_1\rangle + \sin\theta_{12}\,|\nu_2\rangle\,, \tag{24}$$

the observation (survival) probability of the electron neutrino at a distance R is expressed as

$$P_{\text{ee}}^{\text{vac}} = 1 - \sin^2(2\theta_{12})\sin^2\left(\delta m_{12}^2\,\frac{R}{2E}\right). \tag{25}$$

Since $P_{\text{ee}}^{\text{vac}}$ is averaged over the dimensions of the neutrino source and over the neutrino energy, at distances greater than the oscillation length $L = 4\pi E/\delta m_{12}^2$ it is the average value of the electron neutrino flux that is detected:

$$P_{\text{ee}}^{\text{vac}} = 1 - \frac{1}{2}\sin^2(2\theta_{12})\,. \tag{26}$$

The oscillatory behavior of the neutrino in a medium changes owing to its interaction with electrons, since all the neutrinos of three flavors $(\nu_{\text{e}}, \nu_\mu, \nu_\tau)$ interact with an electron via the neutral current, but the electron neutrino experiences an additional interaction via the charged current. As a result, the oscillation amplitude is defined by the mixing angle in matter:

$$\sin^2(2\theta_{\text{m}}) = \frac{\sin^2(2\theta_{12})}{\left[\cos(2\theta_{12}) - Z\right]^2 + \sin^2(2\theta_{12})}\,, \tag{27}$$

where

$$Z = \frac{2\sqrt{2}\,G_{\text{F}}n_{\text{e}}E_\nu}{\delta m_{12}^2}\,. \tag{28}$$

The parameter Z describing the difference between the scattering amplitudes for ν_{e} and ν_μ, ν_τ depends on the Fermi constant G_{F}, on the local electron density n_{e}, and on the neutrino energy E_ν. The mixing angle and oscillation length vary depending on the neutrino energy and electron density, thus manifesting the emergence of the MSW effect [14–18].

8. Measured solar neutrino spectra and fluxes and the LMA-MSW oscillation solution

Figure 9 displays the regions of possible values of the oscillation parameters δm_{12}^2 and θ_{12}, obtained from experiments with solar neutrinos [54, 55]. Experiments with the latter led to five versions of oscillation solutions. One region corresponded to a small mixing angle (SMA), $\delta m_{12}^2 \sim 10^{-5}\ \text{eV}^2$ and $\tan^2\theta_{12} \sim 10^{-3}$, and was determined

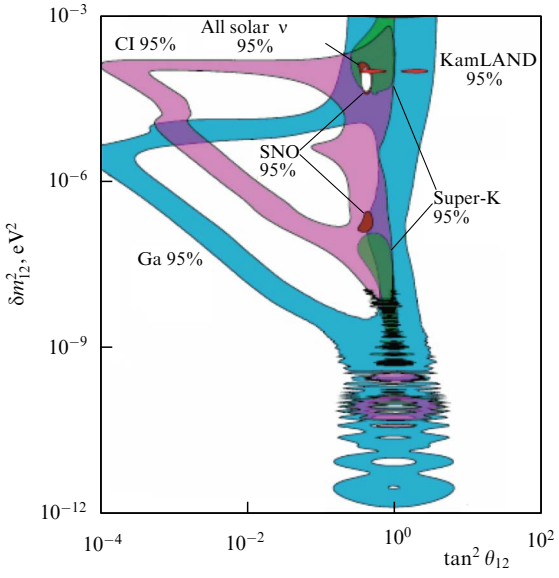

Figure 9. The regions of oscillation parameters resolved by different experiments within the mixing scheme of two neutrinos. (Taken from Ref. [54].)

by the intersection of regions permitted by the Cl–Ar and Ga–Ge experiments. The other four regions were found for a large mixing angle ($\tan^2\theta_{12} \sim 1$): VAC (vacuum) — $\delta m^2_{12} \sim 10^{-11}$ eV^2, when the oscillation length is comparable to the distance from Earth; QVO (quasi-vacuum oscillations) — $\delta m^2_{12} \sim 10^{-9}$ eV^2; LOW — $\delta m^2_{12} \sim 10^{-7}$ eV^2, and LMA — $\delta m^2_{12} \sim 10^{-4}$ eV^2. Upon obtaining the results of the SNO experiment, all other oscillation solutions, with the exception of LMA and LOW ones, were discarded.

It should be noted that before the result of KamLAND was obtained, the spin-flavor precession model, related to the neutrino magnetic moments and their interaction with the solar magnetic field, was in better agreement with the experimental data than any one of the oscillation solutions. The registration of a deficit of reactor neutrinos by the KamLAND experiment clearly revealed the LMA oscillation solution for antineutrinos to be valid.

Finally, the Borexino experiment, performed with a precision of 1%, observed no change in the 'day–night' counting rate of ^{7}Be-neutrinos. This permitted excluding the LOW oscillation solution, which corresponds to $\delta m^2_{12} \sim 10^{-7}$ eV^2, without invoking data from the KamLAND reactor experiment, i.e., without assuming *CPT*-conservation in the neutrino sector [70].

Joint analysis of the results of experiments with solar neutrinos yields the values of $\delta m^2_{12} = 5.2^{+1.6}_{-0.9} \times 10^{-5}$ eV^2 and $\tan^2\theta_{12} = 0.468^{+0.039}_{-0.03} \times 10^{-3}$, if the neutrino fluxes from SHP11(GS98) SSM [20] are used. Inclusion of the KamLAND data on reactor antineutrinos results in a significant enhancement of the precision for δm^2_{12}: $\delta m^2_{12} = 7.5^{+0.16}_{-0.24} \times 10^{-5}$ eV^2 and $\tan^2\theta_{12} = 0.457^{+0.033}_{-0.025} \times 10^{-3}$.

The measurement data on solar neutrino fluxes compared to theoretical predictions of SHP11(GS98) SSM are presented in Table 5.

Table 5. Measured solar neutrino fluxes and results of calculations of these fluxes in SHP11(GS98) SSM [24].

Type of ν	Dimensionality of ν flux	Experiment	SHP11(GS98) model	P_{ee}*
pp	10^{10} cm^{-2} s^{-1}	$6.02(1^{+0.003}_{-0.01})$	$5.98(1 \pm 0.006)$	0.56 ± 0.07
pep	10^8 cm^{-2} s^{-1}	$1.63(1 \pm 0.21)$	$1.44(1 \pm 0.012)$	0.62 ± 0.17
^{7}Be	10^9 cm^{-2} s^{-1}	$4.84(1 \pm 0.05)$	$5.00(1 \pm 0.07)$	0.51 ± 0.07
^{8}B	10^6 cm^{-2} s^{-1}	$5.33(1 \pm 0.026)$	$5.58(1 \pm 0.13)$	0.33 ± 0.018
CNO	10^8 cm^{-2} s^{-1}	$\leqslant 7.7$ (у.д. 95%)	$5.24(1 \pm 0.23)$	—

* P_{ee} is the measured fraction of electron neutrinos.

Figure 10 depicts the observation probability of electron neutrinos as a function of the neutrino energy for the LMA-MSW solution. High-energy ^{8}B-neutrinos are produced in the region of high electron density, which corresponds to $Z \gg \cos(2\theta_{12})$ and $\theta_m \approx \pi/2$, in accordance with expression (27). As a result, a neutrino emanates from the Sun in the form of a second mass state $\approx |\nu_2\rangle$. The registration probability of the electron neutrino on Earth is given by $|\langle\nu_2|\nu_e\rangle|^2 = \sin^2\theta_{12}$. The remaining part of the neutrino flux manifests itself as the flux of ν_μ- and ν_τ-neutrinos, and it also contributes to (ν, e)-scattering via the Z-boson exchange. However, the (ν, e)-scattering cross section, which is due to the neutral current, is about one seventh the magnitude of that for the charged current.

The SNO and Super-Kamiokande experiments provided a 3% accuracy in measurements of the ^{8}B-neutrino flux. The

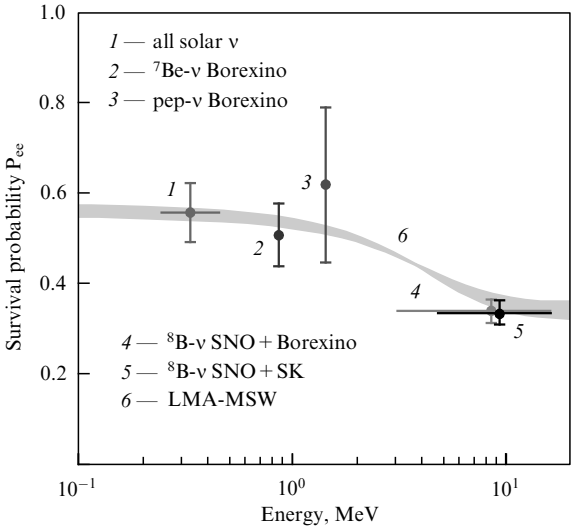

Figure 10. Survival probability of the electron neutrino for the LMA-MSW solution [for the ^{8}B(R)-distribution]. The width of the curve corresponds to the 1σ error in oscillation parameters. The results are shown for experiments with solar neutrinos. (Taken from Ref. [21].)

determined survival probability of an electron ^{8}B-neutrino amounted to $P_{eeB} = 0.33 \pm 0.018 \approx \sin^2\theta_{12}$.

Regarding neutrinos of low energies, $Z \ll \cos(2\theta_{12})$, their oscillations in the Sun proceed like those in a vacuum, and the observation probability of an electron neutrino is determined by expression (26), which quite accurately describes pp-neutrino oscillations: $P_{ee}(pp) = 0.56 \pm 0.07 \approx 1 - (1/2)\sin^2(2\theta_{12})$.

The behavior of the $P_{ee}(E)$ dependence in the region of mutual influence of vacuum oscillations and oscillations in matter is sensitive to nonstandard neutrino interactions, when the neutrino–electron coupling constants depend on the neutrino flavor or even when the flavor changes under (ν, e)- and (ν, N)-interactions. Therefore, it is important to improve the measurement accuracy of P_{ee} for monochromatic ^{7}Be-neutrinos ($E_\nu = 0.862$ MeV) and pep-neutrinos ($E_\nu = 1.44$ MeV).

9. Near-term outlook

Three neutrino detectors, namely SAGE, Kamiokande, and Borexino, continue to be in operation. For over 20 years, measurements performed by SAGE nave been based on the radiochemical method, and, half of the events registered here are caused by pp-neutrinos. Long-term measurements provide the possibility of searching for the dependence of the neutrino counting rate on time.

Super-Kamiokande can be expected to achieve further improvement of the accuracy in determining the ^{8}B-neutrino flux starting from a lower (~ 3.5 MeV) threshold.

Borexino will improve its results for pep- and CNO-neutrinos, and it will be capable of measuring the pp-neutrino flux in the nearest future.

In 2014, measurements should start with the scintillation detector SNO+. The muon flux at Borexino is two orders of magnitude larger than that at the depth of the SNO+ location, so, respectively, the background related to decays of ^{11}C nuclei will be reduced. This gives rise to hopes that signals from CNO-neutrinos will be extracted.

A significant enhancement in the measurement accuracy of solar neutrino fluxes should be expected if the LENA (Low Energy Neutrino Astrophysics) scintillation detector with a mass of 50 kt will be constructed [71].

The lower registration threshold of liquid scintillation detectors based on hydrocarbons is determined by the β-activity of the radiocarbon ^{14}C. The most important task consists in creating neutrino detectors containing no carbon and exhibiting a low registration threshold. Detectors based on liquid noble gases, such as xenon, argon, and neon are the most promising. The Xenon, LUX (Large Underground Xenon), and EXO (Enriched Xenon Observatory) detectors have already revealed their capabilities in experiments searching for the scattering of dark matter particles on nuclei and for double β-decay. For the registration of solar neutrinos, the detector mass must be increased by a factor of several hundred. This is proposed to be realized in the CLEAN (Cryogenic Low Energy Astrophysics with Noble gases) [72] and XMASS (Xe MASSive ν-detector) projects [73].

10. Conclusion

Soon, half a century will have passed since the first solar neutrinos were registered. At the same time, the problem of the solar neutrino deficit has arisen. Today, we know that the observed solar neutrino fluxes are determined both by vacuum oscillations and by neutrino oscillations in matter. Owing to experiments with solar neutrinos, the oscillation parameters θ_{12} and δm^2_{12} have been found.

Real-time detectors have been applied in measurements of ^{8}B-, ^{7}Be-, and pep-neutrino fluxes, and constraints have been imposed on the CNO-neutrino flux, which are only 1.5–2.0 times larger than theoretical SSM predictions.

The task for the next generation of neutrino detectors consists in realizing precise measurements of the spectra of recoil electrons for all solar neutrinos. This will result in a better understanding of the solar structure, processes taking place in the Sun, and the possible contribution from nonstandard neutrino interactions altering both the mechanism of neutrino oscillations in matter and the shape of recoil electron spectra.

The high level on record of purification of the scintillator achieved in the Borexino experiment gives rise to hope that the background problems at low energies, related to natural and artificial radioactivity, can be resolved. The most important experimental tasks are to increase the detector mass and to create detectors lacking in ^{14}C.

The detectors of solar neutrinos that are already in operation or are under construction turn out to be efficient for resolving other physical problems, such as the registration of geoneutrinos (KamLAND, Borexino), searching for neutrinoless double beta-decay (KamLAND-Zen, SNO+, Borexino), and searching for dark matter particles (XMASS, CLEAN) and neutrino oscillations to the sterile state [SOX (Short distance neutrino Oscillations with BoreXino), KamLAND–CeLAND].

This work is supported by RFBR grant 13-02-01199.

References

1. Pontecorvo B *Sov. Phys. JETP* **6** 429 (1958); *Zh. Eksp. Teor. Fiz.* **33** 549 (1957)
2. Pontecorvo B *Sov. Phys. JETP* **7** 172 (1958); *Zh. Eksp. Teor. Fiz.* **34** 247 (1958)
3. Maki Z, Nakagawa M, Sakata S *Prog. Theor. Phys.* **28** 870 (1962)
4. Cleveland B T et al. *Astrophys. J.* **496** 505 (1998)
5. Hirata K S et al. *Phys. Rev. Lett.* **63** 16 (1989)
6. Abdurashitov J N et al. (SAGE Collab.) *Phys. Rev. C* **80** 015807 (2009)
7. Kaether F et al. *Phys. Lett. B* **685** 47 (2010)
8. Hosaka J et al. (Super-Kamiokande Collab.) *Phys. Rev. D* **73** 112001 (2006)
9. Abe K et al. (Super-Kamiokande Collab.) *Phys. Rev. D* **83** 052010 (2011)
10. Aharmim B et al. (SNO Collab.) *Phys. Rev. C* **72** 055502 (2005)
11. Aharmim B et al. (SNO Collab.) *Phys. Rev. Lett.* **101** 111301 (2008)
12. Gribov V, Pontecorvo B *Phys. Lett. B* **28** 493 (1969)
13. Bilen'kii S M, Pontecorvo B *Sov. Phys. Usp.* **20** 776 (1977); *Usp. Fiz. Nauk* **123** 181 (1977)
14. Wolfenstein L *Phys. Rev. D* **17** 2369 (1978)
15. Wolfenstein L *Phys. Rev. D* **20** 2634 (1979)
16. Mikheev S P, Smirnov A Yu *Sov. J. Nucl. Phys.* **42** 913 (1985); *Yad. Fiz.* **42** 1441 (1985)
17. Mikheyev S P, Smirnov A Yu *Nuovo Cimento C* **9** 17 (1986)
18. Mikheev S P, Smirnov A Yu *Sov. Phys. JETP* **64** 4 (1986); *Zh. Eksp. Teor. Fiz.* **91** 7 (1986)
19. Abe S et al. (The KamLAND Collab.) *Phys. Rev. Lett.* **100** 221803 (2008)
20. Bellini G et al. (Borexino Collab.) *Phys. Rev. Lett.* **107** 141302 (2011)
21. Bellini G et al. (Borexino Collab.) *Phys. Rev. Lett.* **108** 051302 (2012)
22. Bethe H A *Phys. Rev.* **55** 434 (1939)
23. Haxton W C, Serenelli A M *Astrophys. J.* **687** 678 (2008); arXiv:0805.2013
24. Serenelli A M, Haxton W C, Peña-Garay C *Astrophys. J.* **743** 24 (2011); arXiv:1104.1639
25. Stonehill L C, Formaggio J A, Robertson R G H *Phys. Rev. C* **69** 015801 (2004)
26. Grevesse N, Sauval A J *Space Sci. Rev.* **85** 161 (1998)
27. Serenelli A M, Basu S, Ferguson J W, Asplund M *Astrophys. J.* **705** L123 (2009)
28. Bethe H, Peierls R *Nature* **133** 532 (1934)
29. Pontecorvo B, Chalk River Laboratory Report PD-205 (1946)
30. Lee T D, Yang C N *Phys. Rev.* **104** 254 (1956)
31. Wu C S et al. *Phys. Rev.* **105** 1413 (1957)
32. Bahcall J N, Davis R (Jr.) *CERN Courier* **40** (6) 17 (2000); *Publ. Astron. Soc. Pacific* **112** 429 (2000); astro-ph/9911486
33. Kuz'min V A *Sov. Phys. JETP* **22** 1051 (1966); *Zh. Eksp. Teor. Fiz.* **49** 1532 (1965)
34. Anselmann P et al. (GALLEX Collab.) *Phys. Lett. B* **285** 376 (1992)
35. Hampel W et al. (GALLEX Collab.) *Phys. Lett. B* **447** 127 (1999)
36. Altmann M et al. (GNO Collab.) *Phys. Lett. B* **616** 174 (2005)
37. Abdurashitov J N et al. (SAGE Collab.) *Phys. Lett. B* **328** 234 (1994)
38. Giunti C, Laveder M *Phys. Rev. C* **83** 065504 (2011); arXiv: 1006.3244
39. Abazajian K N et al., arXiv:1204.5379
40. Gavrin V N et al., arXiv:1006.2103
41. Fukuda Y et al. (Super-Kamiokande Collab.) *Phys. Rev. Lett.* **81** 1562 (1998)
42. Ahmad Q R et al. (SNO Collab.) *Phys. Rev. Lett.* **87** 071301 (2001)
43. Ahmad Q R et al. (SNO Collab.) *Phys. Rev. Lett.* **89** 011301 (2002)
44. Aharmim B et al. (SNO Collab.) *Phys. Rev. C* **88** 025501 (2013)
45. Lozza V (for SNO+ Collab.), arXiv:1201.6599
46. Eguchi K et al. (KamLAND Collab.) *Phys. Rev. Lett.* **90** 021802 (2003)
47. Abe S et al. (KamLAND Collab.) *Phys. Rev. C* **84** 035804 (2011); arXiv:1106.0861
48. Gando A et al. (KamLAND-Zen Collab.) *Phys. Rev. Lett.* **110** 062502 (2013)
49. Gando A et al., arXiv:1309.6805
50. Arpesella C et al. (Borexino Collab.) *Phys. Lett. B* **658** 101 (2008)
51. Arpesella C et al. (Borexino Collab.) *Phys. Rev. Lett.* **101** 091302 (2008)
52. Derbin A V *Phys. Atom. Nucl.* **73** 1935 (2010); *Yad. Fiz.* **73** 1987 (2010)

53. Borexino Experiment, http://borex.lngs.infn.it
54. Beringer J et al. (Particle Data Group) *Phys. Rev. D* **86** 010001 (2012)
55. Nakamura K (Particle Data Group) *J. Phys G Nucl. Part. Phys.* **37** 075021 (2010)
56. Gonzalez-Garcia M C, Maltoni M, Salvado J *JHEP* (05) 072 (2010)
57. Bellini G et al. (Borexino Collab.) *Phys. Rev. D* **82** 033006 (2010)
58. Bellini G et al. (Borexino Collab.) *Phys. Rev. C* **81** 034317 (2010)
59. Bellini G et al. (Borexino Collab.) *Phys. Lett. B* **696** 191 (2011)
60. Bellini G et al. (Borexino Collab.) *Phys. Rev. D* **85** 092003 (2012)
61. Bellini G et al. (Borexino Collab.) *Phys. Rev. D* **88** 072010 (2013)
62. Beacom J F, Vogel P *Phys. Rev. Lett.* **83** 5222 (1999)
63. Joshipura A S, Mohanty S *Phys. Rev. D* **66** 012003 (2002)
64. Grimus W et al. *Nucl. Phys. B* **648** 376 (2003)
65. Montanino D, Picariello M, Pulido J *Phys. Rev. D* **77** 093011 (2008)
66. Beda A G et al. *Phys. Part. Nucl. Lett.* **10** 139 (2013); *Pis'ma Fiz. Elem. Chastits At. Yadra* **10** 217 (2013)
67. Auerbach L B et al. (LSND Collab.) *Phys. Rev. D* **63** 112001 (2001)
68. Schwienhorst R et al. (DONUT Collab.) *Phys. Lett. B* **513** 23 (2001)
69. Bellini G et al. (Borexino Collab.) *JHEP* (08) 038 (2013); arXiv: 1304.7721
70. Bellini G et al. (Borexino Collab.) *Phys. Lett. B* **707** 22 (2012)
71. Wurm M et al. *Astropart. Phys.* **35** 685 (2012)
72. McKinsey D N, Coakley K J *Astropart. Phys.* **22** 355 (2005)
73. Abe K et al. (XMASS Collab.) *Nucl. Instrum. Meth. Phys. Res. A* **716** 78 (2013); arXiv:1301.2815